SAND2017-5760C

Analytical and Experimental Study of Measuring Enthalpy in Geothermal Reservoirs with a Downhole Tool

Xuhua Gao[1], Sasha Egan[2], William C. Corbin[3], Ryan F. Hess[3], Grzegorz Cieslewski[2], Avery T. Cashion[2], Roland N. Horne[1]

[1] Dept. of Energy Resources Engineering, Stanford University
[2] Sandia National Laboratories Geothermal Research Department
[3] Sandia National Laboratories Advanced Materials Laboratory

Keywords

Chloride concentration, downhole enthalpy, feed zone, tool, sensor, solid-state, reference electrode, high temperature, real-time

ABSTRACT

Downhole measurements of enthalpy could provide a better understanding of the performance of geothermal reservoirs and a more accurate estimation of the amount of available thermal energy than surface measurements. However, it is difficult to measure downhole enthalpy in two-phase flow from multiple feed zones. In this work, an analytical model to calculate downhole enthalpy based on chloride concentration measurement was developed. Both two-phase flow and multiple feed zones are considered in the model. An experimental study was conducted to investigate the feasibility of measuring the concentration of the chloride tracer in two phase flow by utilizing a new tool currently being developed by Sandia National Laboratories which is designed to selectively measure the chloride concentration at high temperatures and pressures in real-time. The experimental results obtained by the study are compared with simulation results from ANSYS Fluent, and both results support the key assumption made in the analytical model. The experimental results also validate the functionality of a new type of internal solid-state, high temperature and pressure reference electrode which has been designed for the extreme environments commonly observed in active geothermal reservoirs.

1. Introduction

Wellhead measurements of enthalpy and mass flow rate are routine monitoring procedures in geothermal fields. Due to wellbore heat loss, measurement of surface enthalpy provides incomplete information about the wellbore and the reservoir, especially during the early testing phases of reservoir development. Measurement of enthalpy downhole would allow for better understanding of the reservoir condition and so would be of great practical significance.

Enthalpy of single-phase flow can be obtained directly from measurement of temperature. However, geothermal fluid is often in two-phase flow in the wellbore and the reservoir, and flowing steam fraction would be required to determine the total enthalpy of steam and liquid.

Sandia National Laboratories is a multimission laboratory managed and operated by National Technology and Engineering Solutions of Sandia, LLC., a wholly owned subsidiary of Honeywell International, Inc., for the U.S. Department of Energy's National Nuclear Security Administration under contract DE-NA0003525.

Measuring or calculating flowing steam fraction downhole is not trivial due to the velocity difference between the gas phase and the liquid phase. Atalay (2008) introduced a method to measure gas velocity and void fraction with fiber optics. Spielman (2003) and Juliusson et al (2006) proposed that resistivity measurement with sufficient resolution could also be used to determine gas velocity and void fraction. In both methods, the flowing steam fraction is calculated from gas velocity, liquid velocity and void fraction. Both methods are only applicable in bubble flows and require other equipment to measure liquid velocity at the same time.

The tracer dilution technique can be applied to measure the liquid mass flow rate and the steam mass flow rate using ionic tracers in the liquid phase and vapor tracers in the steam phase respectively. Precisely metered injection of the tracers is required in this technique (Hirtz et al. 1993). For vapor phase tracers, it is difficult to determine the amount of tracer gas dissolved in the liquid phase, which is a major drawback of this method (Lovelock, 2001). In addition, it is necessary to consider the chemical cost of injection and the precipitation of inorganic ion tracers in the pipe.

Gao et al. (2017) proposed a model to calculate downhole enthalpy based on chloride concentration. With a single feed zone, chloride mass balance and total mass balance of steam and liquid are applied to calculate downhole flowing steam fraction and enthalpy, as shown in Equations (1)-(4).

$$d(Cl \cdot q_l) = 0 \tag{1}$$

$$d(\dot{m}) = d(\rho_l \cdot \frac{q_l}{1-x}) = 0 \tag{2}$$

$$x = 1 - \frac{q_{ldownhole}\rho_l}{\dot{m}} \tag{3}$$

$$h_t = (1-x)h_l + xh_s \tag{4}$$

where Cl is chloride concentration, q_l is volumetric flow rate of the liquid phase, $\dot{m}$ is total mass flow rate, ρ_l is the density of liquid phase, x is flowing steam fraction, $q_{ldownhole}$ is downhole volumetric flow rate of the liquid phase, h_t is total flowing enthalpy, h_l is the enthalpy of liquid water, and h_s is the enthalpy of steam.

In the case of multiple feed zones, Gao et al. (2017) demonstrated that liquid flow rate from the feed zone could be obtained by assuming the chloride concentration of the liquid from the feed zone is measurable at the inlet of the feed zone. Figure 1 shows a schematic of the layout of tools in the well.

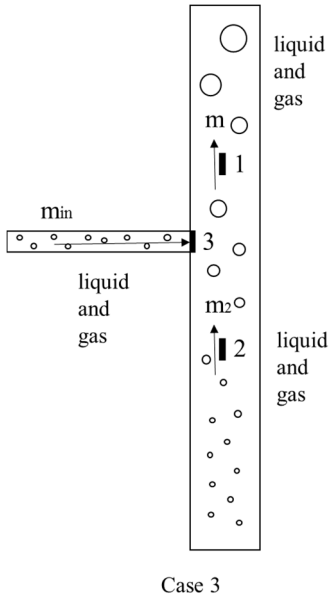

Figure 1: A schematic of the layout of tools in the well

The small black rectangles in Figure 1 represent the tools for chloride concentration measurement. The concentration measured by device 3 is the key parameter. Chloride mass balance is applied to calculate liquid flow rate using the concentrations measured by device 1, 2, and 3 in Figure 1, as illustrated by Equation (5)-(6).

$$q_{lin} \cdot Cl_{in} + (q_l - q_{lin}) \cdot Cl_{below} = q_l \cdot Cl_{above} \tag{5}$$

$$q_{lbelow} = q_l - q_{lin} \tag{6}$$

where q_{lin} is volumetric flow rate of the liquid from the feed zone, Cl_{in} is the chloride concentration of the liquid from the feed zone (measured by device 3), q_l is total volumetric flow rate of the liquid phase (i.e. the liquid flow rate above the feed zone), Cl_{below} is the chloride concentration of the liquid below the feed zone (measured by device 2), Cl_{above} is the chloride concentration of the liquid above the feed zone (measured by device 1), and q_{lbelow} is volumetric flow rate of the liquid phase below the feed zone. Note that q_{lin} is the only unknown in Equation (5) and can be calculated. However, the model has trouble in determining the steam flow rate and the enthalpy with multiple feed zones.

This paper describes a modification and enhancement of the method proposed by Gao et al. (2017) in the following aspects:

- A new model is proposed to calculate steam flow rate from the feed zone in the case where multiple feed zones exist, which allows for estimation of the enthalpy from each feed zone. Multiple feed zones are common in geothermal fields, so this modification enhances the practical application of the approach.
- Gao et al. (2017) showed only an analytical model, while in this paper an experimental study of the downhole tool is included along with discussion on the development, fabrication of a new solid-state reference electrode, and initial test results demonstrating the ability of the new tool to measure chloride concentration in two-phase wells.

- The assumption that the chloride concentration measured at the inlet of the feed zone can represent the exact concentration of the liquid from the feed zone plays an important role in the model and influences the accuracy of the model. Experimental study was conducted to examine the validity of this important assumption.
- Computational fluid dynamic (CFD) simulation of the feed zone behavior was carried out using ANSYS Fluent and compared to the experimental results.

2. Analytical Model

In two-phase geothermal wells with multiple feed zones, it is difficult to determine the specific amount of liquid and steam contributed by each feed zone. In Section 1, it was explained that liquid contribution from the feed zone can be obtained by measuring chloride concentration of the liquid from the feed zone. The model discussed in this section focuses on calculating steam flow rate from the feed zone.

Measurement of temperature is much easier than measurement of gas velocity and void fraction. It is feasible to measure the temperature of the in-flowing geothermal fluid from the feed zone, and then apply the energy balance to calculate flow rate from the feed zone.

Saturated steam enthalpy and liquid enthalpy can be determined by measuring temperature or pressure. Due to the existence of geothermal gradient, different feed zones often have different temperatures and steam enthalpies. This difference can be harnessed, and an energy balance can be applied to determine the amount of steam from each feed zone.

The energy balance indicates that the total energy in the fluid above the feed zone equals the energy in the fluid coming from the feed zone and the energy in the fluid below the feed zone, as shown in Equation (7).

$$m_{lbelow}h_{l0} + m_{sbelow}h_{s0} + m_{lin}h_{lin} + m_{\sin}h_{\sin} = m_{labove}h_{l1} + m_{sabove}h_{s1} \tag{7}$$

Variable descriptions from Equation (7) are shown in Table 1.

Table 1: Variables in Equation (7)

Variables		Above the feed zone	From the feed zone	Below the feed zone
Steam	Mass flow rate	m_{sabove}, known from the single feed zone model proposed by Gao et al. (2017)	$m_{\sin}$	m_{sbelow}
	Enthalpy	h_{s1}, known from temperature or pressure measurement	h_{sin}, known from temperature measurement at the feed zone	h_{s0}, known from temperature or pressure measurement
Liquid	Mass flow	m_{labove}, known from	m_{lin}, known from	m_{lbelow}, known from

rate	the single feed zone model proposed by Gao et al. (2017)	the Equation (5)-(6)	the Equation (5)-(6)
Enthalpy	h_{l1}, known from temperature or pressure measurement	h_{lin}, known from the temperature measurement at the feed zone	h_{l0}, known from temperature or pressure measurement

From Table 1, $m_{\sin}$ and m_{sbelow} are the only two unknown variables in Equation (7), and the mass balance of steam gives that:

$$m_{sbelow} + m_{\sin} = m_{sabove} \tag{8}$$

Combining Equation (8) and Equation (7), the steam mass flow rate from the feed zone and the steam mass flow rate below the feed zone can be solved. m_{sbelow} and m_{lbelow} can be used to calculate flowing steam fraction and enthalpy below the feed zone:

$$x = \frac{m_{sbelow}}{m_{lbelow} + m_{sbelow}} \tag{9}$$

$$h_t = (1-x)h_{l0} + xh_{s0} \tag{10}$$

Figure 2 shows a roadmap of the method.

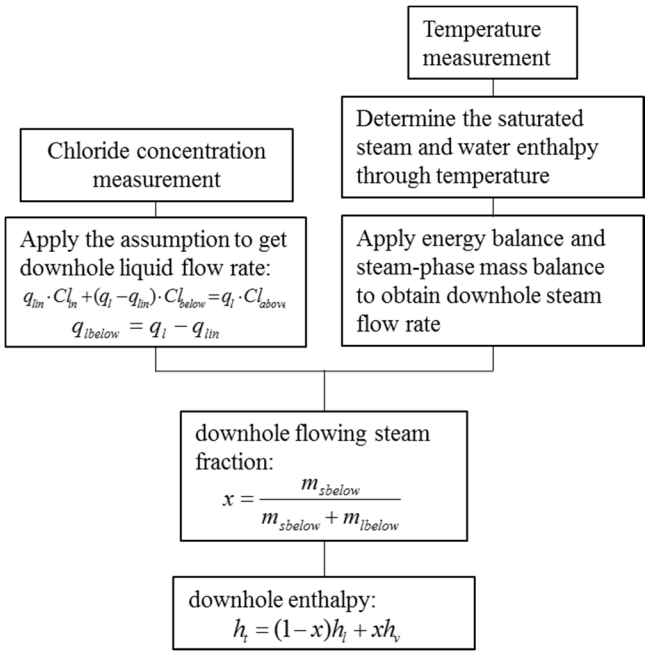

Figure 2: Roadmap of calculating enthalpy with multiple feed zones

An example of applying energy balance and mass balance to calculate enthalpy with multiple feed zones is provided, as shown in Table 2.

Table 2: An example for enthalpy calculation with multiple feed zones

	Surface	Downhole (above feed zone)	Downhole (at the depth of feed zone)	Downhole (below feed zone)
Input	Pressure: 12.55 bar-a; Total mass flowrate: 50kg/s; Steam fraction: 0.419; Chloride concentration: 400g/m^3	Chloride concentration: 300g/m^3; Pressure: 55.06 bar-a;	Chloride concentration: 280 g/m3; Temperature: 260 °C	Chloride concentration: 320 g/m^3; Temperature: 280 °C
Output		Flowing steam fraction: 0.3214; Enthalpy: 1701 kJ/kg;	Steam fraction: 0.1571; Enthalpy: 1396 kJ/kg	Steam fraction: 0.4304 Enthalpy: 1901 kJ/kg

In the example, total mass flow rate above the feed zone is 50 kg/s with a total flowing enthalpy of 1701 kJ/kg. The steam fraction above the feed zone is 0.3214. The liquid mass flow rate from the feed zone is 16.9 kg/s, and the liquid mass flow rate below the feed zone is 17.1 kg/s. The temperature measured at the feed zone is 260 °C, indicating a steam enthalpy of 2796.6 kJ/kg and a liquid enthalpy of 1134.8 kJ/kg. The temperature measured below the feed zone is 280 °C, indicating a steam enthalpy of 2779.8 kJ/kg and a liquid enthalpy of 1236.7 kJ/kg. Steam flow rates from and below the feed zone are calculated to be 3.15 kg/s and 12.92 kg/s respectively. The total flowing enthalpy below the feed zone is 1901 kJ/kg.

3. Development and Assembly of the Downhole Tool

The original tool developed at Sandia National Laboratories is a wireline tool containing a ruggedized electrochemical sensor for real-time tracer concentration measurement (Cieslewski et al. 2016; Corbin et al. 2017). New developments with the tool allow for function specific configurations of the ion-selective sensing elements. Specifically, the tool was configured for chloride concentration measurements and was scaled down to a lab manageable size for the laboratory setting. The lab scale tool was 29.3 cm in length and 2.65 cm in diameter. The tool consists of three electrodes: a chloride-ion selective electrode (Cl-ISE), a reference electrode and a graphite electrode.

3.1 A New Reference Electrode

Electrochemical measurement accuracy is highly dependent upon the performance of the reference electrode. The electrochemical behavior of silver/silver-chloride reference electrodes is well characterized and therefore a common choice when performing Nernstian sample analysis. Commercial liquid solution silver/silver-chloride reference electrodes are a proven technology that has been used for many years in autoclave housed electrochemical measurements. Typically,

a central silver wire is coated in silver/silver-chloride and suspended in a liquid electrolyte solution with a semi-porous frit separating the electrolyte from the sample liquid. For high-pressure environments, a bellows system is necessary to equalize pressure on either side of the frit to prevent the part from exploding or dislodging the frit. Additionally, a section of the reference electrode that cannot withstand the high temperature/high pressure environment is mounted outside the autoclave. The system described herein may provide comparable performance to a commercial silver/silver-chloride reference electrode while being more robust, simpler to assemble, entirely solid-state, and can be directly integrated into high-temperature tools.

It was recognised early in the project life cycle that a stable reference electrode, which was capable of performing while being subjected to the high temperatures and pressures present in most geothermal environments, would be required. Performing reliable chemical tracer sensing and enthalpy measurements within high-temperature and high-pressure aqueous systems is not a straightforward proposition. The stability of internal reference electrodes under the harsh conditions imposed, and will continue to pose, major measurement challenges. The current method of performing these measurements is to physically separate the electrochemically active elements into an ‘internal’ and ‘external’ classification.

An internal reference electrode has the potential sensing, electroactive element, maintained at the system temperature and pressure. This allows for the working electrode, counter electrode and reference electrode, to exist in a relative state of thermodynamic equilibrium. An external reference electrode has the electroactive element maintained outside of the high temperature and pressure system, at ambient conditions, with the communicating electrolyte bridge being actively air or water-cooled. This places the two systems at a non-isothermal condition and therefore they are not at equilibrium due to the thermal diffusion phenomena experienced along the cooled electrolyte bridge. The sacrifice made by adopting the external method is loss of precision and the increased need for copious amounts of error correction data.

Since the development project requires a relatively high degree of precision it is desirable to have an internal reference electrode that behaves reversibly, accurately, and predictably. Unfortunately, most electroactive elements will not withstand an aqueous environment in excess of 200°C. The Advanced Materials Laboratory (AML) in cooperation with the Geothermal Research and Development group at SNL, have worked together to develop an internal solid-state reference electrode for which preliminary test results indicate predictable behavior up to 225°C.

3.1.1 Material Synthesis

A spherical graphite powder with a particle distribution in the submicron to micron range was plated with elemental silver by the reduction of silver nitrate. The solution, during the drop-wise reduction, was agitated to ensure the graphite particles were uniformly plated. The silver plated graphite powder was then vacuum filtered, washed with cold distilled water, and then dried in an oven. The silver plated graphite particles were re-suspended in a solution of silver nitrate where a second reduction was performed using potassium chloride. The solution, during the drop-wise reduction, was again agitated to ensure a uniform coating of silver chloride over the particles.

The silver and silver chloride coated graphite particles were vacuum filtered, washed with cold distilled water, and then oven dried. This theoretically creates a conductive graphite core, plated with metallic silver, covered with a silver chloride shell (Figure 3).

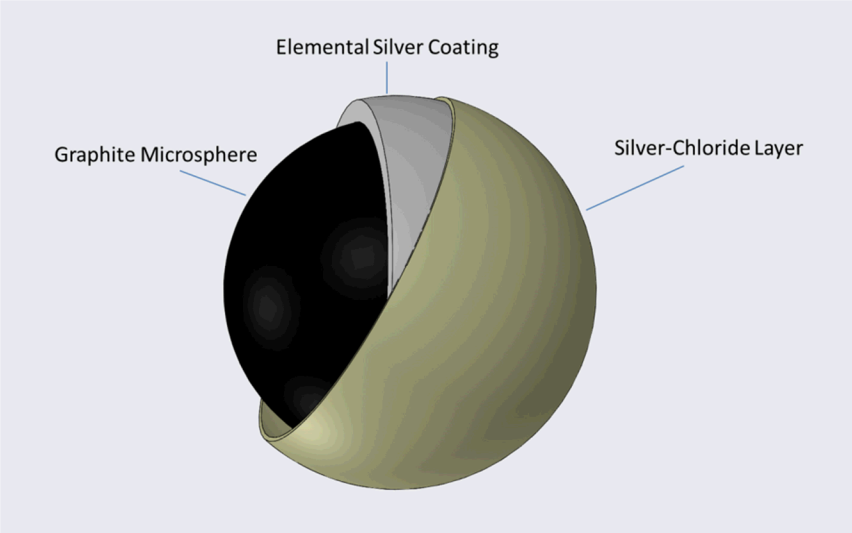

Figure 3: Diagrammatic representation of synthesized particles. The central conductive graphite sphere is coated with a silver layer and subsequently a silver chloride layer.

3.1.2 Pellet Fabrication

A layer of 250 milligrams of the silver and silver chloride coated graphite powder is placed in a pellet die followed by a layer of 250 milligrams of pure potassium chloride. The two components are pressed into a single bimodal pellet at approximately 5 tons with a dwell time of 8 hours (Figure 4).

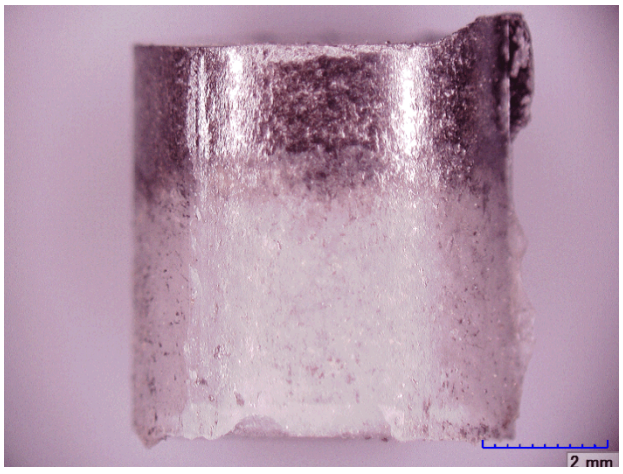

Figure 4: An image of the bimodal pellet after pressing.

3.1.3 Electrode Assembly

210 millimeters of conductor were cut from 0.275 millimeter diameter, bar stock material. The ends of the bar stock were squared and polished, ending with a 0.3 micron chromium oxide abrasive polish. A layer, approximately 0.3 mm in thickness, of Cotronics Duralco 124 high temperature conductive epoxy was applied to a clean, polished, end of the conductor and the silver coated graphite end of the pellet is attached to the conductor. This assembly was cured at 170°C overnight. The pellet attached to the conductor is ground down to the diameter of the conductor removing all oversized regions which would create any possible overhangs. The pellet and conductor were potted using Cotronics Duralco 124 high temperature conductive epoxy in a high density alumina tube with the exception of a small area in the center of the potassium chloride end of the pellet. The assembly was again cured overnight at 170°C. The alumina tube was ground down until 5 mm of void space remained above the potted pellet. The void above the pellet was filled with Cotronics Resbond 904 zirconia based adhesive. The assembly was placed under vacuum to 200 mbar to remove any air pockets between the pellet and the zirconia adhesive. This vacuum was cyclically performed until no further reduction in volume was observed whereby a maximum density was achieved. The zirconia adhesive was allowed to cure at room temperature for twenty-four hours before being placed in an oven at 170°C for one hour to ensure a fully cured bond and to drive off any accumulated moisture. The entire assembly was covered in Zeus Duel-Shrink PTFE/FEP shrink tubing and placed in an oven at 342°C, until the shrink tube completely encased the assembly.

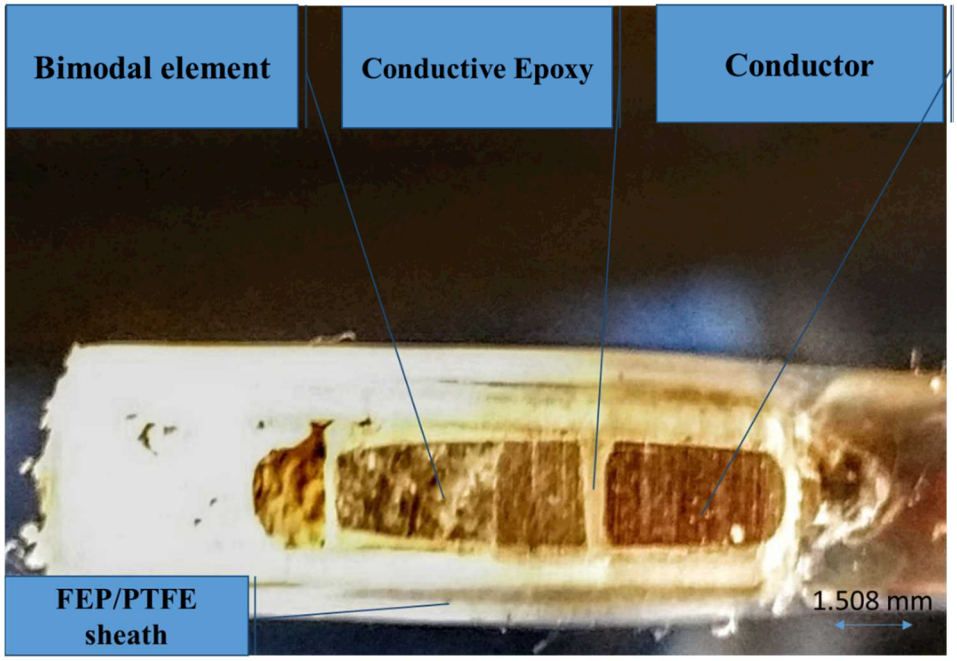

Figure 5: A second generation solid-state reference electrode similar to one used during the current study.

3.1.4 Initial Evaluation Run

The prototype assembly was trial tested at high temperature and pressure against a commercial reference electrode in an initial evaluation run (Figure 6).

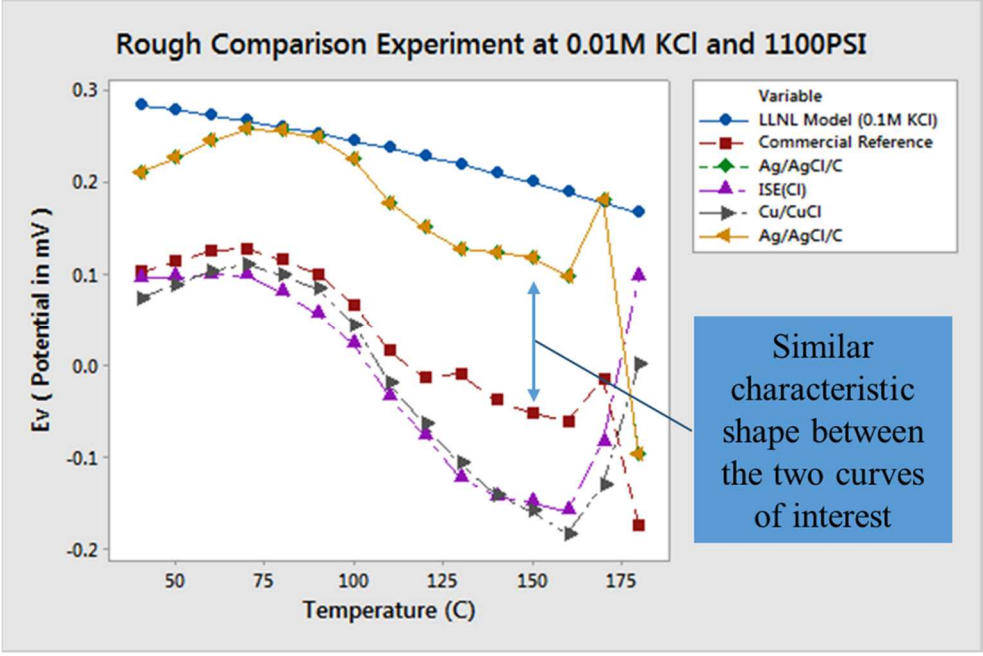

Figure 6. A comparison of the reference electrode performance over temperature sweep to other technologies. The rough comparison of the prototype response followed the commercial reference response closely in shape with an offset. The offset is not important in differential electrochemistry measurements as a calibration curve will be necessary at each temperature regardless of the electrode formulation.

The evaluation run simultaneously tested the prototype internal solid-state reference electrode at high temperature and pressure while using an external commercial reference electrode as a control. The response from both units was recorded and compared during the evaluation with a positive result. The response from the internal solid-state reference electrode closely mirrored that of the external commercial reference with only a 100 millivolt offset throughout the temperature sweep which ranged from ambient (approximately 21°C) to 225°C at a constant pressure of 7.58MPa. This was the limit of the current testing equipment.

3.2 Tool Assembly

The scaled down benchtop version of the tool used in the current study required three sensing elements to be constructed and assembled. A chloride ion-selective electrode was fabricated using the methods already outlined (Cieslewski et al. 2016; Corbin et al. 2017). A solid-state reference electrode was fabricated using the method outlined in Section 3.1.3. Lastly, a graphite rod was turned down by lathe to a diameter of 6.35 millimeters which was then center-bored with a 2.26 millimeter bit. A #4 stainless steel machine screw was threaded into the bore as a conductive contact point. The solid-state reference electrode, ion-selective electrode, and graphite were then inserted into a lower Teflon grommet (gromit) designed to space the electrodes evenly apart. The electrodes were covered with a PVC toolbody which was mated to the lower grommet. A four conductor wireline was stripped back to expose the inner conductors and a single conductor was attached with copper tape to each electrode. The void space within the tool body was filled with non-conductive electronics potting epoxy to secure all of the interior elements. The tool body was then secured with a threaded upper Teflon grommet. The epoxy compound was allowed to cure for twenty-four hours prior to running calibration tests. A diagram of the assembled tool can be seen in Figure 8.

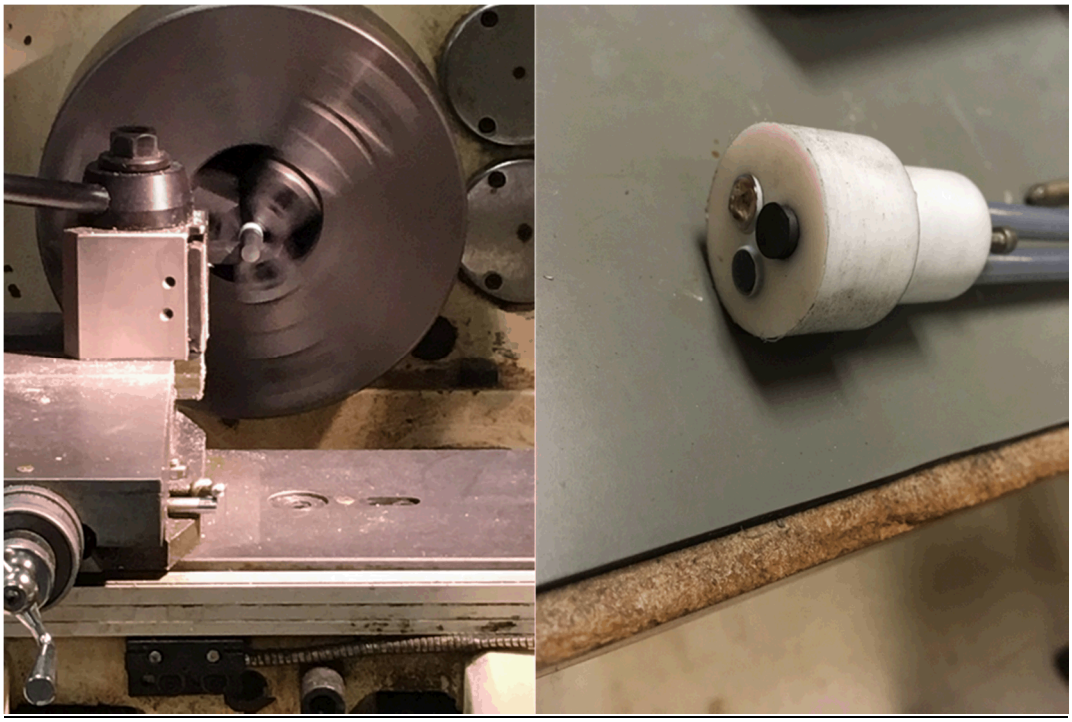

Figure 7: Prototype construction for testing in multiphase flow chamber. (Left) Lathe turning of graphite rod for ground reference and potentiostat measurements (Right) Assembly of three electrode system; Ion selective electrode, solid state bimodal pellet reference electrode, and graphite ground reference electrode.

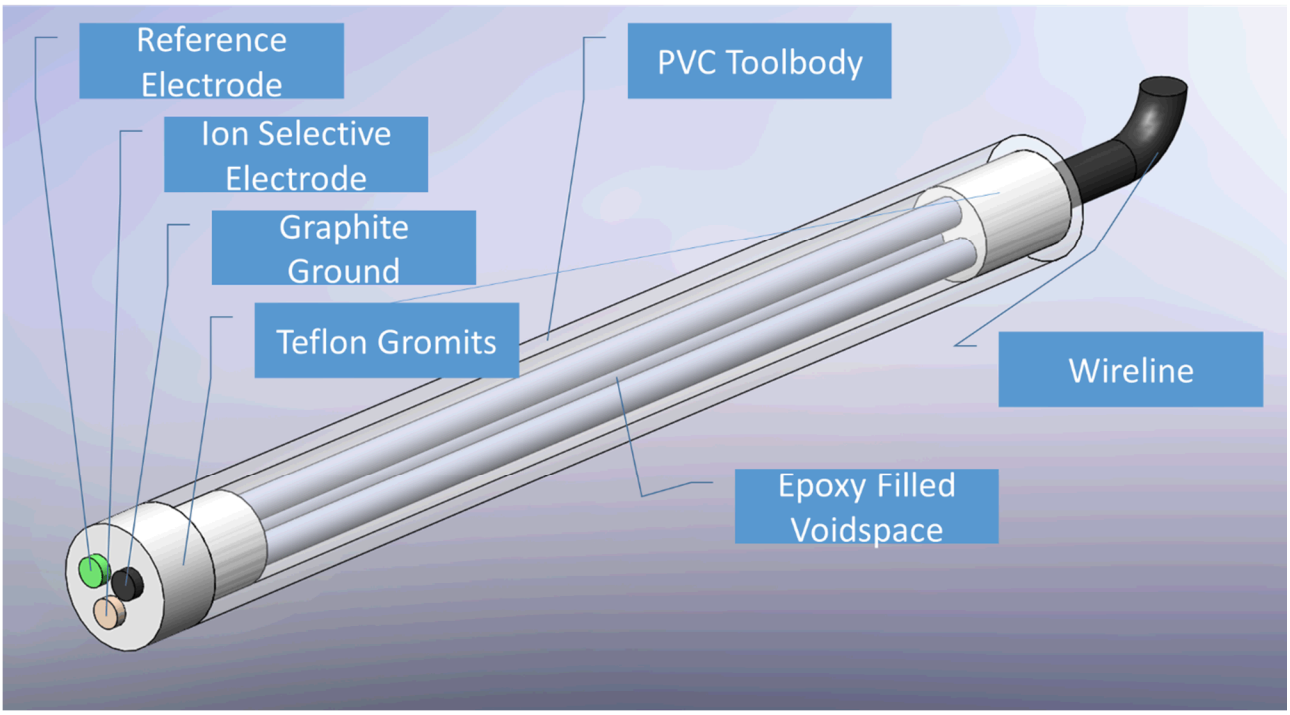

Figure 8: A cut-away diagram of the benchtop version of the tool used in this study - Assembled

4. Experimental Study of Chloride Concentration Measurement in Two-Phase Flow

4.1 Calibration of the Tool

In the experiment, the potential difference between the Cl-ISE and the reference electrode was measured in sodium chloride solution with different concentrations for calibration purpose. Calibration experiments were conducted at both Sandia National Laboratories and Stanford Geothermal Laboratory. In Figure 9, the blue dots represent data collected at Sandia, and the red dots represent data collected at Stanford.

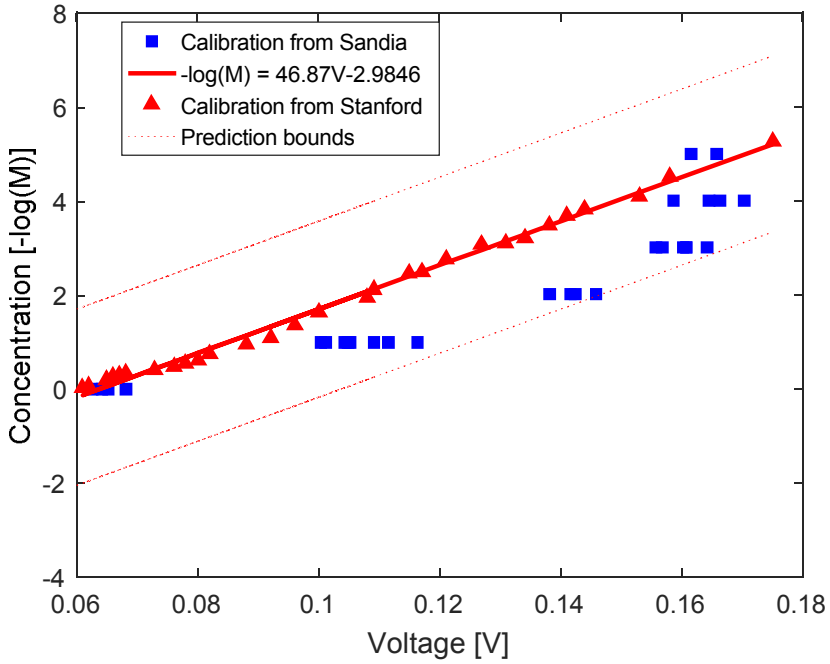

Figure 9: Calibration of the tool

The calibration from Sandia included four test groups and provided distributions of measurements and prediction bounds at different chloride concentration levels. The distribution provided by Sandia has an overall standard deviation of 0.03584 Volts. The time required to reach equilibrium is longer at lower concentrations than at higher concentrations. In tap water, the settling time was approximately 1 hour, which gave the lowest variance of between 5.3 to 5.7 millivolts. Another group of calibrations was done at Stanford. The tool was immersed in saturated sodium chloride solution for 24 hours before the experiment to allow for rehydration of the tool. As we can see from Figure 9, both calibrations were completed with a well-defined linear relationship, and the calibration result obtained at Stanford was consistent with that obtained at Sandia.

By fitting the calibration results, a relationship between the chloride concentration and the voltage was found:

$$-\log(M) = 46.87 \cdot Voltage - 2.9846 \tag{11}$$

where M is the concentration of chloride in mol/L, and the unit of *Voltage* is in Volts. The regression has an R^2 of 0.99.

This relationship was used in later experiments for chloride concentration measurement.

4.2 Measurement of Downhole Chloride Concentration in Two-Phase Flow

An artificial well that can flow two-phase fluid was used for chloride concentration measurement. Figure 10 shows a photo of the well.

Figure 10: Photo of the well

The well is 5.5 inch in diameter and 71.3 inch in height. Water was pumped into the well and was circulated through the system. An in-house compressed air source supplied air to the system. Both water and air enter the well from the bottom after going through a flow mixer. The well is equipped with three injection ports to simulate feed zones.

The tool was placed into the well from the top. A photo of the tool in two-phase bubble flow is shown in Figure 11.

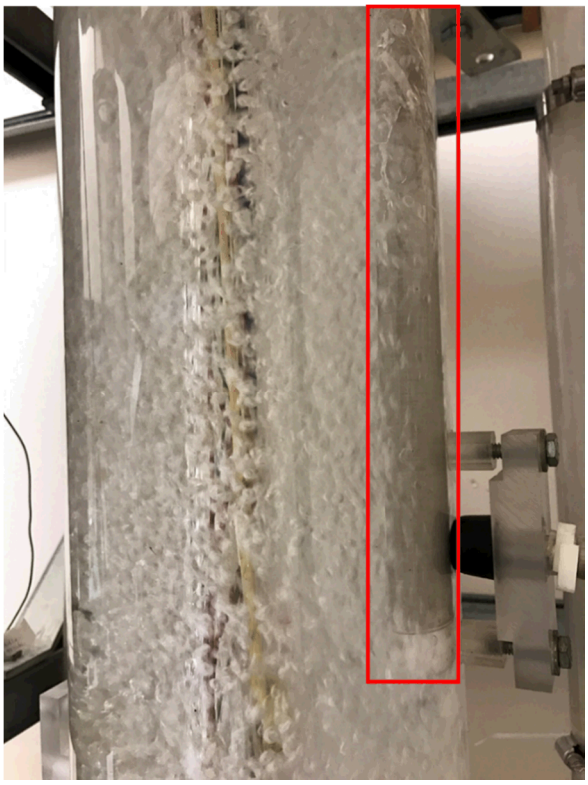

Figure 11: Photo of the tool in two-phase flow

Chloride concentration was measured in the flowing well in both single-phase (liquid) flow and two-phase flow. The liquid flow speed was about 0.3 m/s, and the liquid flow rate was about 6.7 kg/s. The experiments were conducted with constant liquid flow rate but varying gas flow rate, ranging from 1 standard cubic feet per minute (SCFM) to 6 SCFM.

The chloride concentration in the liquid phase was increased incrementally from 0.115 mol/L to 0.832 mol/L. Data of chloride concentration measured under each gas flow rate is shown in Figure 12. The unit slope line in Figure 12 indicates the actual chloride concentration of the liquid phase, and deviation from the unit slope means measurement error occurs at the corresponding point. As we can see from Figure 12, the measurement data points are relatively consistent with the unit slope line, and measurement in single-phase (liquid) flow is more accurate than that in two-phase flow. It was found that the chloride concentration measured in two-phase flow was slightly higher than that measured in single-phase flow, because the tiny bubbles in two-phase flow increased the voltage between the electrodes of the tool, and thus decreased the apparent chloride concentration obtained from the voltage.

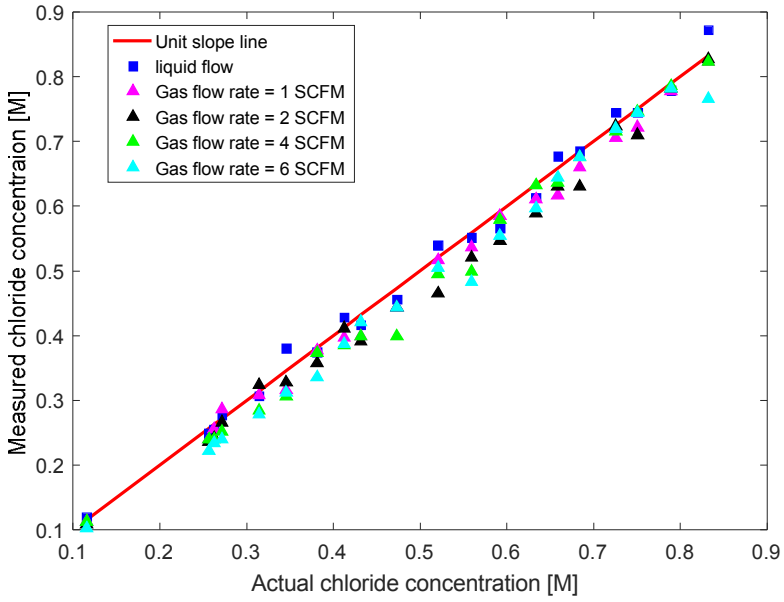

Figure 12: Measurement of chloride concentration in single-phase and two-phase flows

Figure 13 shows average relative errors in chloride concentration measurements with different gas flow rates. Although a trend can be observed that the relative error increases with the gas flow rate, the average relative error with high gas flow rate (6 SCFM) is still acceptable (less than 7%).

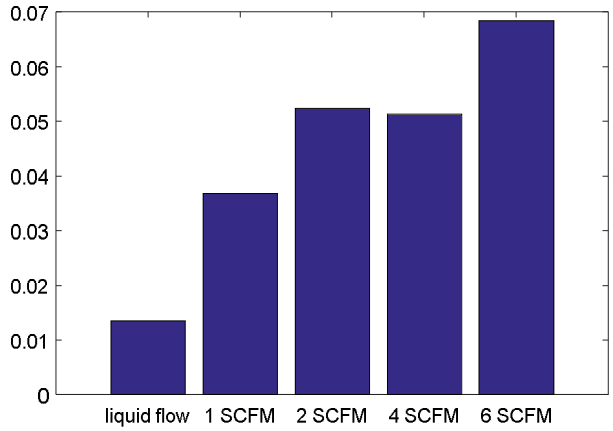

Figure 13: Average relative error with different gas flow rates

The effect of gas phase on the measurement error is expected to be smaller when the gas is in the form of slug or annular flow where lower quantities of small diameter gas bubbles are entrained within the flow.

In conclusion, the tool is capable of measuring chloride concentration in two-phase flow and providing basis for enthalpy calculation in the analytical model.

5. Measurement of Chloride Concentration of Liquid from the Feed Zone

As elaborated in Section 1 and 2, our analytical model relies on a key assumption that the chloride concentration measured at the inlet of the feed zone can represent the actual chloride concentration of the liquid from the feed zone. This assumption is important for determining downhole enthalpy with multiple feed zones, because measuring the chloride concentration from the feed zone allows us to calculate the liquid flow rate from the feed zone based on chloride mass balance. It is necessary to study the mixing behavior of the fluid from the feed zone with the fluid in the well.

5.1 Observation of the Mixing Zone Using Experimental and Simulation Methods

In order to understanding the influence of the in-flowing fluid from the feed zone and visualize the mixing procedure, both experiments and simulation were carried out, and the results compared.

In the experiment, the in-flowing fluid was dyed with red color, so that it could be distinguished from the fluid in the well. The colored fluid was injected from the port into the well. In the simulation, the in-flowing fluid has higher chloride concentration than the fluid in the well. The visualization results achieved through experimental method and simulation method are compared in Figure 14.

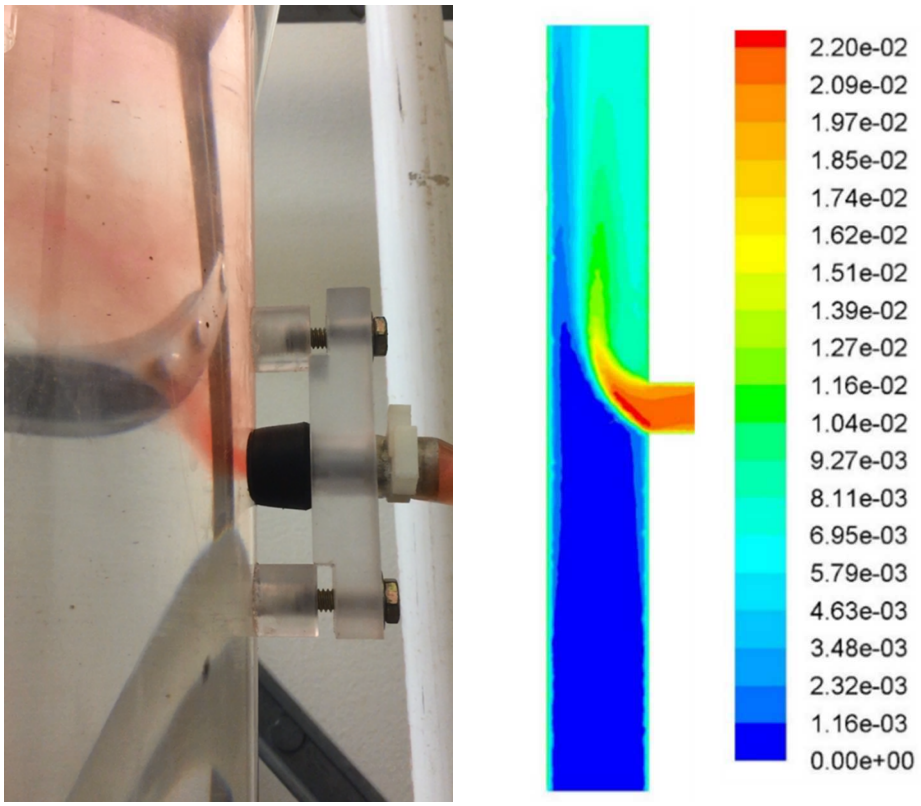

Figure 14: Comparison between experimental result and simulation result

The color bar in Figure 14 shows mass fraction of sodium chloride in the fluid. It can be seen from Figure 14 that the mixing zone in the experiment result has a similar shape with the mixing zone in the simulation result. Both experiment and simulation indicate that the concentration at

the inlet of the feed zone is very close to the exact concentration of the liquid from the feed zone. The concentration distribution is quantified through experiment discussed in Section 4.2.

The distribution of fluid velocity and air volume fraction based on the simulation is shown in Figure 15 and Figure 16, respectively.

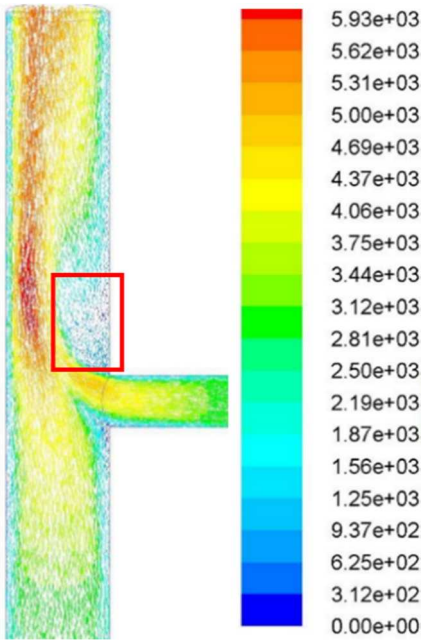

Figure 15: Distribution of fluid velocity. The unit of the color bar is mm/s.

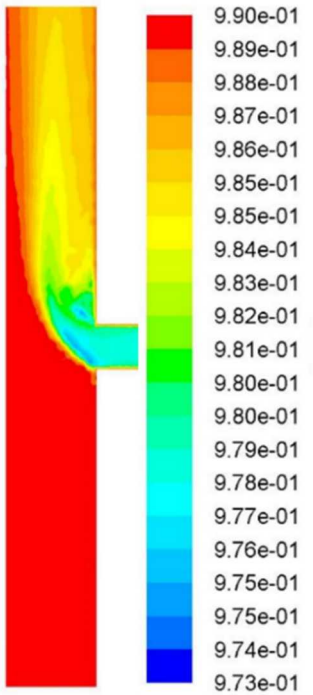

Figure 16: Distribution of air volume fraction

It can be seen from Figure 15 that the flow around the mixing zone is turbulent, and a vortex formed in the area marked by the red rectangle in Figure 15.

5.2 Distribution of Chloride Concentration in the Mixing Zone

The experiment discussed in this part was also conducted in the artificial well shown in Figure 10. Liquid flowing from the bottom was tap water with very low chloride concentration, while liquid injected through the port had high chloride concentration. The experiments consisted of two groups. In the first group, the chloride concentration of the injection liquid was 0.23 mol/L, and in the second group, the chloride concentration of the injection liquid was 0.61 mol/L. In both groups, chloride concentration was measured at different distances from the inlet (from 0 to 5cm) to study the distribution of chloride concentration in the mixing zone. Because the flow in the mixing zone was turbulent, the measurement token at each distance from the inlet was unstable and displayed a distribution, which is shown in Figure 17-18.

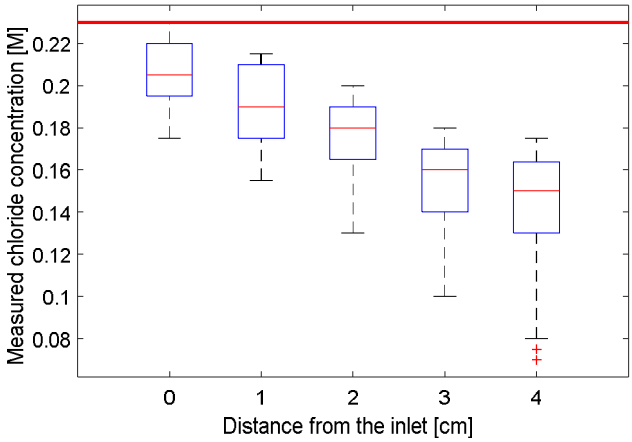

(a) Feed zone concentration 0.23 mol/L

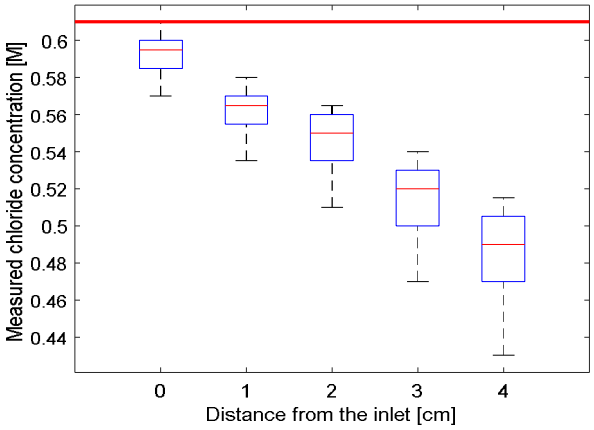

(b) Feed zone concentration 0.61 mol/L

Figure 17: Boxplot of concentration distribution in the mixing zone

The boxplots in Figure 17 shows the mean value, P10 and P90 of the chloride concentrations measured at different distances. Figure 17(a) and 17(b) are based on group 1 and group 2 respectively. As expected, chloride concentrations measured at longer distance from the inlet have lower values and larger variance. The red lines in Figure 17 and Figure 18 indicate the chloride concentrations of the liquid from the feed zone.

Figure 18 shows the estimated distribution of the measurement data.

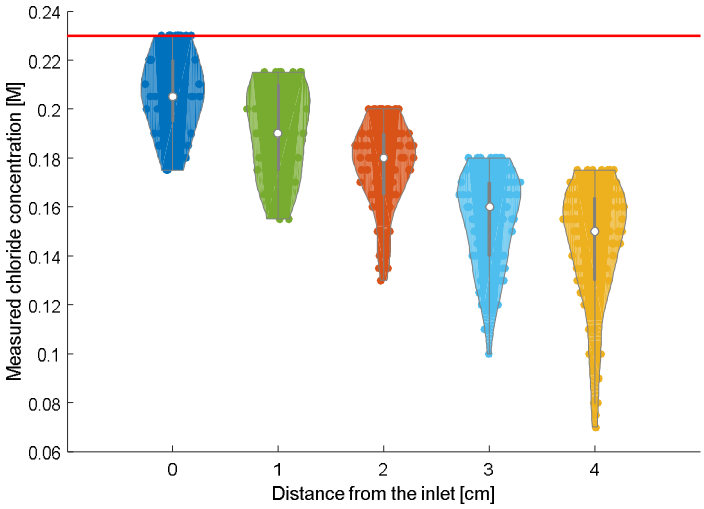

(a) Feed zone concentration 0.23 mol/L

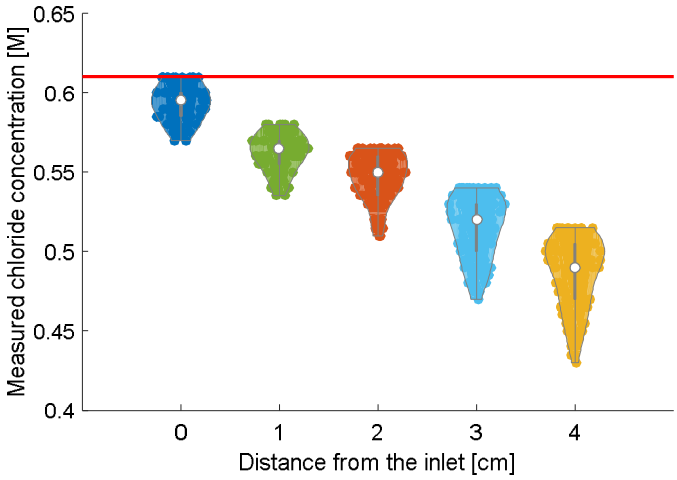

(b) Feed zone concentration 0.61 mol/L

Figure 18: Violinplot of concentration distribution in the mixing zone

As we can see in Figure 17 and Figure 18, the variance of the measurements increase with the distance from the inlet. However, if the tool is placed closely against the wall of the well and the inlet, like shown in Figure 14, it is feasible to obtain the concentration value from the feed zone relatively accurately.

In Figure 17 and Figure 18, the top of the distribution at distance 0 touches the red line, meaning the highest concentration measured is very close to the true concentration of the liquid from the feed zone. Even though in some cases it is hard to align the tool against the wall of the well, we can adjust our measurement based on Figure 17 and Figure 18.

6. Conclusion

(1) A modified analytical model for enthalpy calculation based on chloride concentration measurement is discussed. In the modified model, it is unnecessary to measure gas velocity and void fraction when multiple feed zones exist. Instead, energy balance and chloride mass balance can be applied to calculated downhole flowing enthalpy. This method offers a considerable advantage in making a practical downhole measurement.

(2) Experimental study with the tool developed by Sandia National Laboratories demonstrates that real-time measurement of chloride concentration in two-phase geothermal wells can be achieved, which provides the basis for the analytical model.

(3) A key assumption in the analytical model that chloride concentration of the liquid from the feed is measurable was examined through experimental and simulation methods. The results indicate that the highest measurement at the inlet can represent the chloride concentration of the liquid from the feed zone, which supports the assumption made in the analytical model.

(4) The experimental results have validated the functionality of a new type of internal solid-state, high temperature and pressure reference electrode which has been designed for the extreme environments commonly observed in active geothermal reservoirs.

ACKNOWLEDGEMENT

This project is partially funded by the United States Department of Energy Geothermal Technologies Office (DOE-GTO) and partially funded from internal Sandia National Laboratories funds through the Laboratory Directed Research and Development program (LDRD).

Sandia National Laboratories is a multimission laboratory managed and operated by National Technology and Engineering Solutions of Sandia, LLC., a wholly owned subsidiary of Honeywell International, Inc., for the U.S. Department of Energy's National Nuclear Security Administration under contract DE-NA0003525.

REFERENCES

Atalay, N. "Downhole Enthalpy Measurement in Geothermal Wells with Fiber Optics." Stanford Geothermal Program Report, (2008), SGP-TR-186.

Cieslewski, G., Hess, R. F., Boyle, T. J., and Yelton, W. G. "Development of a Wireline Tool Containing an Electrochemical Sensor for Real-time pH and Tracer Concentration Measurement." *Proceedings*: *Geothermal Resources Council*, Davis, California, CA (2016).

Corbin, W. C., Cieslewski G., Hess R. F., Klamm B. E., Goldfarb L., Boyle T. J., and Yelton W. G. "Development of a Downhole Tool for Measuring Enthalpy in Geothermal Reservoirs." *Proceedings*: *42th Workshop on Geothermal Reservoir Engineering*, Stanford University, Stanford, CA (2017).

Gao, X., Cieslewski, G. and Horne, R. "Development of a Downhole Technique for Measuring Enthalpy." *Proceedings*: *42th Workshop on Geothermal Reservoir Engineering*, Stanford University, Stanford, CA (2017).

Hirtz, P., Lovekin, J., Copp, J., Buck C. and Adams M. "Enthalpy and Mass Flowrate Measurement for Two-Phase Geothermal Production by Tracer Dilution Techniques." *Proceedings*: *18th Stanford Workshop on Geothermal Reservoir Engineering*, Stanford University, Stanford, CA (1993).

Juliusson, E. "An Investigation of Void Fraction And Dispersed-phase Velocity Measurement Techniques." Stanford Geothermal Program Report, (2006), SGP-TR-181.

Lovelock, B. G. "Steam Flow Measurement Using Alcohol Tracers." *Geothermics*, 30, (2001), 641-654.

Spielman, P.B. Coso Operating Co., LLC. "Apparatus and Method for Measuring Enthalpy and Flow Rate of a Mixture." U.S. Patent 6,575,045, 2003.

APPENDIX I

A1 Corrosion Failure Phenomena in Early Prototypes

During the fabrication process, for an early prototype, a semi-porous alumina and zirconia tube was filled with potassium chloride and heated to 800°C in order to render the salt molten. The electroactive element was then placed into the molten salt and the salt was allowed to solidify. This immobilisation method served as both an anchor and the electrolyte bridge for the electroactive element. The electrode was then placed into a one molar potassium chloride solution and connected to a high impedance oscilloscope where the stability of the measured electrochemical potential was evaluated for a time period of between four and seven days. An unsuccessful candidate from the test group would generally be discarded if the recorded potential drifted excessively, erratically, or the element displayed unwanted or unexpected behaviours -- such as a non-standard potential or excessive corrosion.

Due to the corrosive nature of both the fabrication and operational environments, the 316 stainless steel conductors are heat treated for four hours at 170°C, rinsed and wiped with ethyl alcohol, then conditioned at 342°C for one hour. The passivation process on the conductive element was followed by the application of an epoxy barrier coat before the final fabrication step took place.

One of the early prototypes, that failed the initial quality control check and was subsequently rejected, displayed an unusual amount of corrosion. It was desirable to analyse the corroded

element to ascertain where the passivation, and/or fabrication process, failed to adequately protect the conductor.

The failed electrode was encased in two part epoxy and sectioned via a manual grinding process. A series of silicon carbide (60 – 1200 grit) grinding wheels were used to incrementally expose each layer of the sample. As the potassium chloride interior was water soluble a cyanoacrylate adhesive was used to fill in any void spaces which were exposed during the grinding process. The reason for this was an attempt to protect the mechanical integrity of the interior of the sensor during further grinding. Each subsequent layer, as it was exposed, was examined via optical microscopy until the point of origin for the failure and correlative corrosion was established. The sample was then polished using a series of, incrementally decreasing, micron sized particle abrasives. The polishing abrasives were three micron, followed by one micron, crystalline diamond powder, applied respectively, to finish the sample. The polishing abrasives were primarily used to expose the extent of the corrosion network by adding contrast between the respective materials.

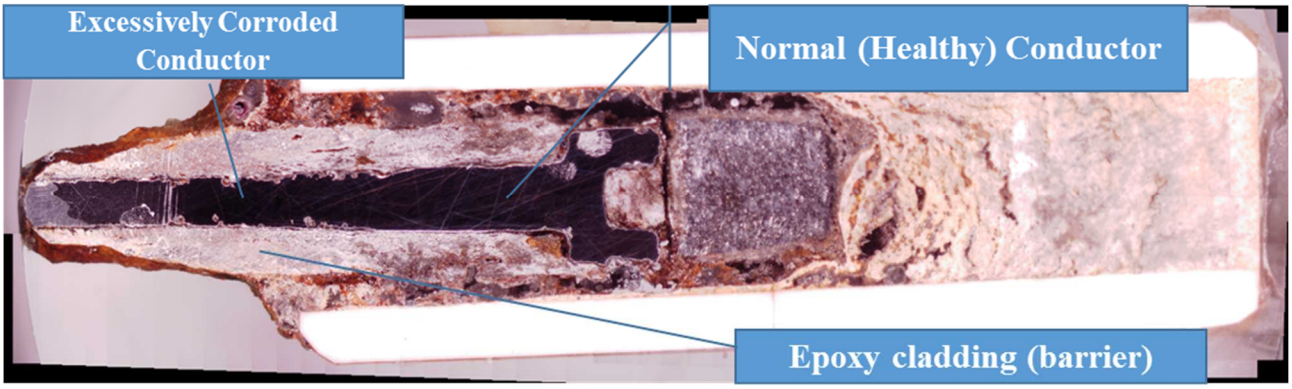

Figure 1A: A bisection of the failed element displayed an unusual patter of corrosion, two distinct regions are evident.

A bisection of the failed electrode displayed an unusual distribution of corrosion near the top of the conductor when it was examined under magnification using a HiRox® digital microscope. Very little corrosion was observed to be occurring within the interior of the electrode or on the lower portion of the conductor despite this having been in intimate contact with a molten potassium chloride environment. However, the upper section of the conductor displayed extensive pitting corrosion and this corrosion appeared to occur upon the conductor in a non-uniform pattern whereby two distinct regions were observed to have developed. A closer examination, at higher magnification, of the actively corroding region of the conductor displayed textbook indications of pitting corrosion. This region, which displayed the most extensive amount of pitting corrosion, was determined to be the most probable point of origin. As a singular point of interest, it was observed that the corrosion occurred symmetrically when revolved about the long axis of the sensor. The observation of the unusual pattern of corrosion and the symmetrical manner in which it affected the conductor assisted in the identification of the mechanism ultimately responsible for the failure of the sensor assembly.

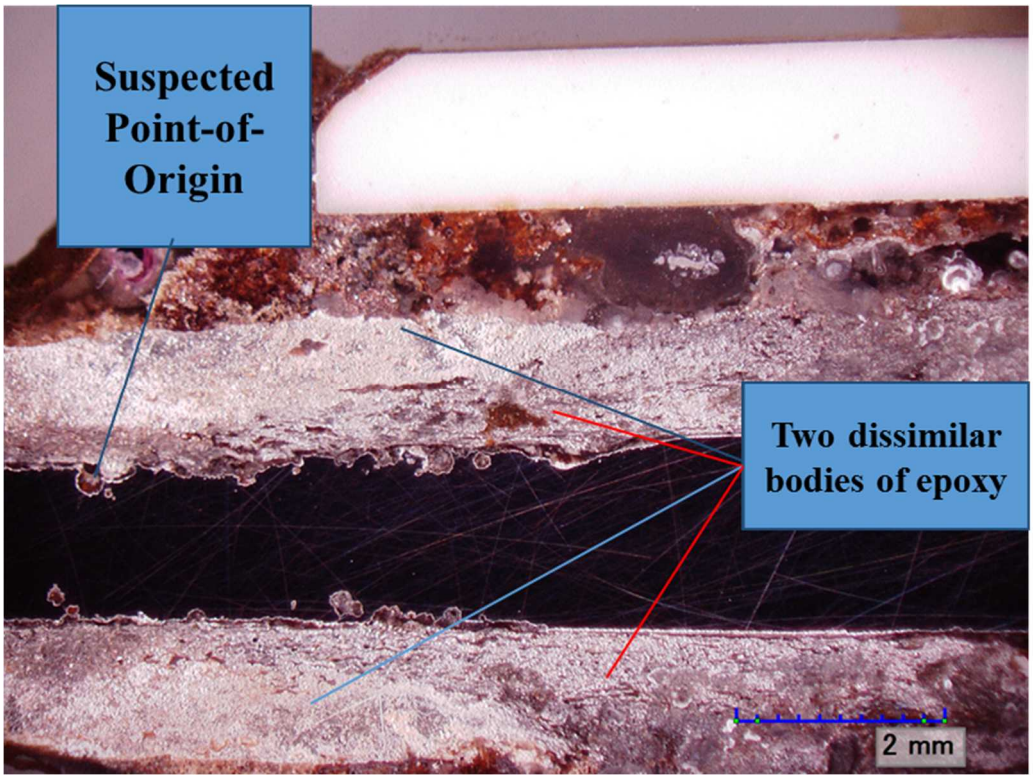

Figure 2A. The region showing the most extensive amount of corrosion was determined to be the point of origin.

In Figure 2A, near the indicated point of origin, two dissimilar bodies in the epoxy cladding were plainly evident. The differing flow patterns between the two bodies indicated that two separate applications of the epoxy cladding had occurred, differing in either times and/or mixture compositions. The interface between these two regions of epoxy was considered the most probable route of infiltration whereby chloride rich solution was drawn up through the interface via capillary action. As the chloride solution corroded the steel, the corrosion products swelled at the interface which caused a partial delamination of the epoxy cladding. The delamination formed a self-propagating crevice which continued to creep down the face of the conductor.

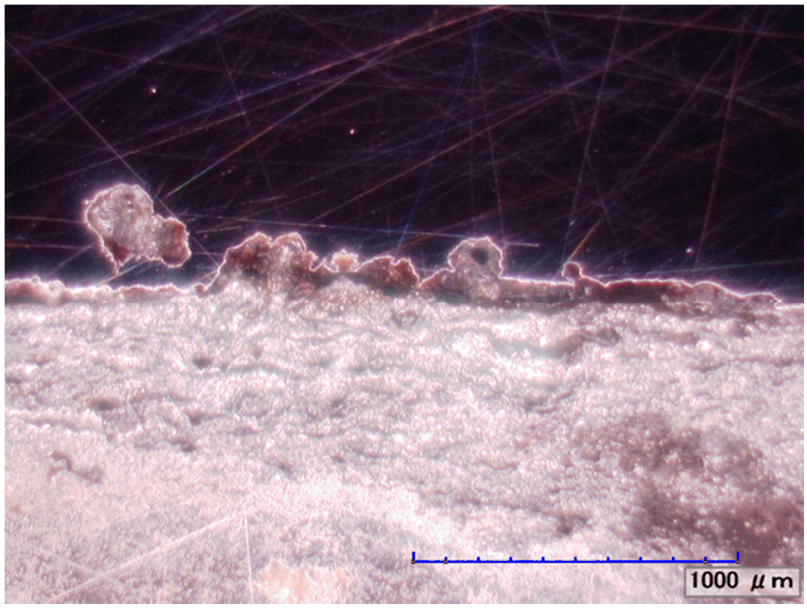

Figure 3A. Two distinct flow patterns indicate an interface between two separate applications of epoxy cladding.

A1.1 Corrosion Mitigation

After completing the analysis of the failed element several recommendations were considered. A thorough passivation procedure was recommended. A thorough passivation process, through a nitric acid bath, prior to the heat treatment is well documented to remove trace iron and manganese from the conductor surface and would improve the corrosion resistance of the conductor element. A possible change of the conductor material, to a material known to be more resistant to chloride corrosion, was also recommended. Lastly, a recommendation that any future design considerations would deprecate all use of a molten potassium chloride assembly process. The final recommendation coincides with the development of the bimodal sensing element which has been showing stability in current evaluations. The bimodal element incorporated the electrolyte bridge with the sensing material via high pressures. This made the sensor much more compact and reduced the exposure of various points susceptible to corrosion failure.